Eur. J. Mineral.
2005, **17**, 703-714

Stavelotite-(La), a new lanthanum-manganese-sorosilicate mineral from the Stavelot Massif, Belgium

HEINZ-JÜRGEN BERNHARDT[1], THOMAS ARMBRUSTER[2], ANDRÉ-MATHIEU FRANSOLET[3] and WERNER SCHREYER[1]*

[1]Institut für Geologie, Mineralogie und Geophysik, Ruhr-Universität, D-44780 Bochum, Germany
[2]Laboratorium für chemische und mineralogische Kristallographie, University of Bern, Freiestr. 3, CH-3012 Bern, Switzerland
[3]Laboratoire de Minéralogie, Université de Liège, Bâtiment B 18, Sart Tilman, B-40000 Liège, Belgium

Abstract: Stavelotite-(La), simplified formula $La_3Mn^{2+}{}_3Cu(Mn^{3+},Fe^{3+},Mn^{4+})_{26}[Si_2O_7]_6O_{30}$, occurs as an accessory opaque mineral in a late quartz vein cross-cutting the deep-purple, highly oxidised manganiferous phyllites of Ordovician age at Le Coreux near Salmchâteau, Belgium. Accompanying minerals are hematite, braunite, hollandite-strontiomelane, kanonaite, Mn-oxides, albite and muscovite. Stavelotite-(La) is trigonal, space group $P3_1$, with a = 11.525(2), c = 33.347(9) Å, V = 3836(1) Å^3 and Z = 3. Its very complex, densely packed crystal structure consists of four different polyhedral layers stacked parallel to the **c**-axis: Layer 1 consists of eight-coordinated distorted cube sites for Mn^{2+} sharing edges with strongly distorted Mn^{3+} polyhedra (tetragonal bipyramids), and also contains one planar square site for Cu^{2+}. Layer 2 has more regular octahedra for Mn^{3+} as well as for the Mn^{4+} required for charge balance, and it contains SiO_4 tetrahedra oriented in one direction. Layer 3 contains additional SiO_4 tetrahedra oriented in two different opposing directions in order to make connection with those of layers 2 and 4, thus forming the $[Si_2O_7]$ groups, and it carries La in eightfold coordination. Layer 4 is of similar architecture as layer 2, but in an inverted position. Layers 1, 2 and 4 are geometrically similar to respective layers in the structure of the mineral långbanite. 65 electron microprobe analyses yielded the following mean composition (Mn valences calculated on the basis of structural data): SiO_2 20.17; TiO_2 0.44; MnO_2 4.83; Mn_2O_3 31.67; MnO 5.99; Al_2O_3 3.30; Fe_2O_3 13.08; Sc_2O_3 1.47; La_2O_3 8.39; Nd_2O_3 3.39; Ce_2O_3 0.44; CaO 0.33; MgO 1.06; CuO 2.11; CoO 0.18; total 96.86 wt.% giving the empirical formula (45 cations, 72 oxygens) $(La_{1.828}Nd_{0.715}Ce_{0.095}Ca_{0.209}Sc_{0.153})_{\Sigma 3.000}$ $Mn^{2+}{}_{2.998}$ $(Cu_{0.941}Mn^{3+}{}_{0.058})_{\Sigma 0.999}$ $(Mn^{3+}{}_{14.183}Fe^{3+}{}_{5.814}Al_{2.298}Ti_{0.195}Sc_{0.604}Mg_{0.933}Co_{0.085}Mn^{4+}{}_{1.973})_{\Sigma 26.085}$ $Si_{11.915}$ O_{72}. Thus, the structural and chemical data are mutually consistent showing all crystallographic positions fully occupied. There are no indications for the presence of hydrogen or other light elements, which were not analysed. Stavelotite-(La) is the first REE silicate mineral containing only large amounts of Mn (with some Fe) as additional cations.

Key-words: new mineral: stavelotite-(La), sorosilicate, new crystal structure, chemical analysis (mineral), Belgian Ardennes.

Introduction

Rare-earth-element(REE)-bearing silicate minerals are copious. Even when concentrating on the element La alone, the mineralogical listings yield some fifty entries. However, in most of these, manganese is but a minor component relative to major elements like Fe, Mg, Al, Na, Ca and Ti. Only the recently found new epidote-group mineral androsite-(La) is an exception, in which considerable amounts of Mn are linked with REE and Si, but also with Ca and Al (Bonazzi *et al.*, 1996). Here we describe a new REE silicate mineral, in which manganese is by far the dominant cation ranging before Si, Fe and the REE, while Al and Ca remain low or very low. Among the REE, surprisingly only La and Nd appear as major elements.

As a second surprise, stavelotite-(La) was found to exhibit a new and enormously complex crystal structure that is related to "the remarkable långbanite structure type" (Moore *et al.*, 1991), except that it is still more complicated.

The mineral name relates to the Stavelot Massif in the Belgian Ardennes Mountains, where stavelotite-(La) appears as a product of late crystallization within a quartz vein. Stavelot is a historical town in eastern Belgium. The mineral and its name were approved by the IMA-Commission on New Minerals and Mineral Names (CNMMN – 2004 – 014). Type material has been deposited at the Mineralogical Collection of the Institut für Geologie, Mineralogie und Geophysik, Ruhr-Universität Bochum, Germany, Catalogue Number 25169. Although the new mineral has thus far no counterpart carrying a dominant

*E-mail: werner.schreyer@ruhr-uni-bochum.de

0935-1221/05/0017-0703 $ 5.40
DOI: 10.1127/0935-1221/2005/0017-0703

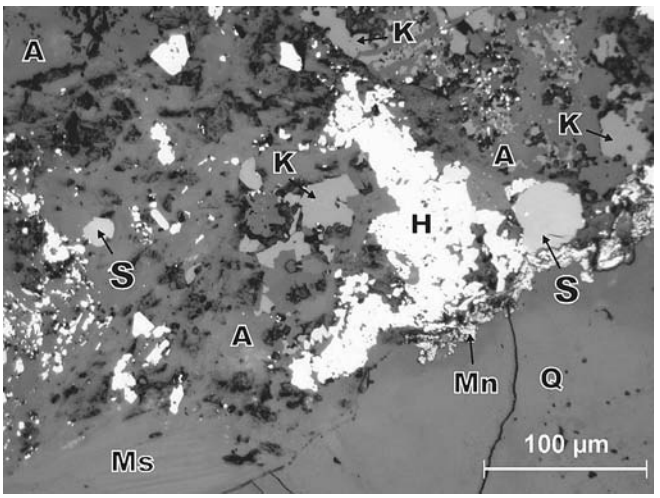

Fig. 1. Reflected-light photograph of enrichment of opaque minerals at the border of albite (A, upper portion) and quartz (Q, lower portion). **S** = stavelotite-(La), H = hematite, K = kanonaite, Mn = Mn-oxides, Ms = muscovite. Thin section Cor 8-2 of sample 25169. Le Coreux, Belgium. In air.

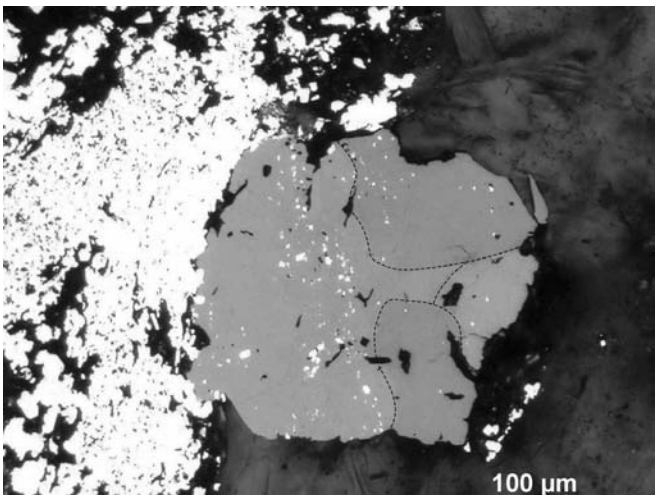

Fig. 2. Reflected-light photograph of irregularly shaped mass consisting of at least four individual single crystals of stavelotite-(La). Grain boundaries are marked faintly by thin black dashes. The high-reflectance mineral to the left and as rare inclusions within stavelotite is hematite. In oil.

RE element other than La, the suffix "-(La)" is required based on CNMMN rules (Nickel & Grice, 1998).

Occurrence

Stavelotite-(La) was found in the same hand specimen (Cor 8, now renumbered as 25169) of a quartz vein, which had already yielded the crystals of end-member ferrian kanonaite recently described by Schreyer *et al.* (2004). Its locality Le Coreux, about 1 km north of Salmchâteau along the western flanks of the Salm river valley, is a well-known occurrence of manganese minerals. It lies in the south-eastern portion of the Stavelot Massif, which represents a Caledonian basement inlier near the northwestern border of the Hercynian Rhenish Massif. The outcrop occurs in the "Les Plattes" Member, a lithostratigraphic unit recently proposed by Verniers *et al*. (2001), and formerly called Middle Salmian or Sm2b. This unit is part of the Ottré Formation, belonging to the Salm Group of Ordovician age. For details of the geological development as well as the crystallization history within the quartz vein, we refer to the paper by Schreyer *et al*. (2004).

The quartz vein sample 25169, about 8 cm in diameter, was collected as a loose boulder in the talus slope of the Le Coreux outcrop, where in steep cliffs deep-purple, highly oxidized phyllites with numerous manganese minerals are exposed. Summaries were presented by Corin (1968), Fransolet *et al*. (1977), Kramm (1982) and Schreyer *et al*. (2001). Macroscopically, the sample consists mainly of milky to colourless quartz with interspersed dark grey to black, irregularly shaped roundish patches in the centimeter range, as well as occasional millimeter-sized yellowish crystals of albite.

Under the petrographic microscope, the dark patches turn out to be complex aggregates of various opaque minerals intergrown with or included in quartz. Even in transmitted light, hollandite-strontiomelane may be recognized by virtue of its needle-like to long prismatic morphology (see Fig. 1 in Schreyer *et al.*, 2001). Blocky, stout, opaque crystals can either be braunite, kanonaite, hematite, Mn-oxides, or even the new mineral stavelotite-(La). Upon closer inspection, kanonaite can occasionally be distinguished from the others by thin transparent peripheries showing dark green to coffee-brown pleochroism (Schreyer *et al*., 2004). Although stavelotite-(La) can be recognized in reflected light by its relatively low reflectance (see later), it was discovered as a special phase only during careful electron microprobe work aimed at locating the most Mn-rich kanonaites (Schreyer *et al*., 2004). This required a multitude of semiquantitative energy dispersive (EDS) reconnaissance analyses on opaque crystals, some of which showed unusually low Si and – most importantly – the lines of La in the spectrum. They turned out to be the of new mineral. Altogether, stavelotite-(La) is but a minor accessory mineral within the quartz vein sample.

In the present paper, we concentrate on one area in thin section Cor 8-2 prepared from sample 25169, where several stavelotite-(La) crystals occur, together with other opaques, along the border of a grain of albite against the surrounding quartz. There, stavelotite-(La) is in association with hematite, braunite, kanonaite, Mn-oxides, quartz, albite and muscovite (partly sericitic). The reflected-light photograph of Fig. 1 shows most of these minerals as well as the characteristic low reflectance of stavelotite-(La), which is only slightly higher than that of kanonaite.

Physical properties

Stavelotite-(La) is megascopically black with a metallic lustre and generally opaque. However, in rare cases of very

Table 1. Spectral reflectance values and measuring conditions for stavelotite -(La) in air and immersion oil.

	Air		Oil			Air		Oil	
λ nm	**R_1 %**	**R_2 %**	**R_1 %**	**R_2 %**	**λ nm**	**R_1 %**	**R_2 %**	**R_1 %**	**R_2 %**
400	15.7	16.5	3.6	4.55	**560**	13.1	13.8	2.85	3.5
420	14.6	15.4	3.3	4.2	**580**	13.0	13.7	2.8	3.4
440	14.1	14.9	3.2	4.0	**589***	13.0	13.7	2.8	3.4
460	14.1	14.5	3.05	3.8	**600**	12.9	13.6	2.8	3.35
470*	13.6	14.4	3.0	3.7	**620**	12.9	13.5	2.8	3.3
480	13.5	14.3	3.0	3.7	**640**	12.9	13.5	2.7	3.25
500	13.3	14.1	2.9	3.65	**650***	12.8	13.4	2.7	3.2
520	13.2	14.0	2.9	3.6	**660**	12.8	13.4	2.7	3.2
540	13.2	14.0	2.9	3.5	**680**	12.8	13.3	2.7	3.2
546*	13.2	13.9	2.9	3.5	**700**	12.8	13.4	2.7	3.2
* COM-wavelengths are interpolated									
Colour values for illuminant C									
x	0.304	0.304	0.302	0.296					
y	0.308	0.310	0.307	0.299					
Y %	13.1	13.85	2.9	3.4					
λ_d	472	476	475	472					
P_e %	3.2	3.0	4.1	7.0					

Mean n at 546 nm: 2.14 ± 0.01

Measuring conditions

Monochromator:	16 homogeneous interference filters (FWHM: *ca*. 10 nm)
Photomultiplier:	Hamamatsu R 3896
Standard:	SiC (Zeiss, no. 878)
Immersion oil:	Zeiss oil corresponding to DIN 58.884 (n_{oil} = 1.5180)
Effective NA:	0.25 in air and oil (plane glass reflector)
Polishing method:	1 μm diamond on lead laps, final buffing with Al_2O_3 in water on cloth

thin cross sections, a dark reddish brown colour was observed in transmitted light, which is probably identical to the indeterminate color of the streak. The new mineral appears as roundish to rectangular, generally equidimensional masses with diameters ranging from about 10 to 160 μm (Fig. 1 and Fig. 2). These masses are either anhedral single crystals or, more often, consist of two or more untwinned individual crystals with different orientations, a feature only recognizable in reflected light under oil immersion by virtue of slightly different reflectances (Fig. 2) and colours. No cleavage or fracturing was observed. Hardness was not determined.

Reflectance curves were determined using a non-commercial automatic spectral microscope reflectometer built at the Ruhr-Universität Bochum. 16 homogeneous interference filters with peak wavelengths between 400 and 700 nm in steps of 20 nm, situated on a wheel are inserted sequentially into the lightpath of a Leitz Orthoplan microscope. First the reflected light intensities for each wavelength are measured on sample and standard using a photomultiplier tube. Then the reflectance and colour values are computed. Results and measuring conditions are summarized in Table 1. In reflected light, stavelotite-(La) is of grey color (dark-grey in oil) and shows very weak to weak bireflectance and very weak pleochroism (only visible in oil). Under crossed polars, it shows very weak anisotropism without colour effects, and complete extinction. Internal reflections are very rare and hardly visible in air, they are rare in oil, weak and brownish.

The density calculated from the structural and chemical data to follow later is 4.489 g/cm^3. Applying the Gladstone-Dale relationship, stavelotite-(La) falls into the category "excellent" as defined by Mandarino (1981). More details will be reported in the section on chemical composition.

Crystal structure

Because no mineral or other crystalline compound was found in the literature to contain similar proportions of the main elements Mn, Si, rare earths and oxygen, a determination of the structural properties of the stavelotite phase had the highest priority in order to understand and define the new phase. Therefore, a crystal of stavelotite-(La), about 100 by 100 by 30 μm in size, was drilled out from thin section Cor 8-2 by our colleague Olaf Medenbach at Bochum, and the structural results are reported first here.

The excavated single crystal of stavelotite-(La) selected for data collection was mounted on a Bruker PLATFORM three-circle goniometer equipped with SMART 1K CCD detector mounted at a crystal to detector distance of 5.4 cm. The data were collected using graphite monochromated Mo*K*α X-radiation and frame widths of 0.3° in ω, with 60 s used to acquire each frame. More than a hemisphere of three-dimensional data were collected. Additional information regarding data collection and structure refinement is given in Table 2. The data were reduced using the program SAINT (Bruker AXS, 1999). A semi empirical absorption-correction based upon the intensities of equivalent reflections was applied (program XPREP (Bruker AXS, 1997)) and the data were corrected for Lorentz, polarization, and background effects. The SHELXTL system of programs

Table 2. Details of X-ray data collection of stavelotite-(La)

Space group	$P3_1$
a , c (Å),	11.525(2), 33.347(9)
V (Å^3)	3836(1)
Z	3
X-ray radiation	Mo$K\alpha$
X-ray power	50 kV, 40 mA
Temperature	293 K
Crystal size	100 × 100 × 30 μm^3
Machine	BRUKER SMART
Collection mode	Half sphere
Exposure time per frame	60 sec.
Upper θ limit	28°
h, k, l limit	15- ≤ h ≤ 15, -12 ≤ k ≤ 14, -42 ≤ l ≤ 35
Reflections measured	22008
Unique reflections	9204
Reflections > 4σ (F)	2839
Absorption correction	Empirical psi-scans
Twinning	50:50 by center of symmetry
R (σ) %	13.32
Number of least square parameters	388
GooF	0.900
R1%, Fo > 4σ(Fo)	10.00
R1%, all data	22.70
WR %(on F^2)	26.76
Highest residual peaks in difference-Fourier map	3 e/Å^3 and –2 e/Å^3

(Bruker AXS, 1998) was used for solution and refinement of the crystal structure. The positions of all cations were located by direct methods and O sites were retrieved from subsequent difference Fourier analyses. The final refinement, applying neutral-atom scattering factors, included atomic positional and isotropic displacement parameters constraint to be equal for each atomic species. The constraints were chosen mainly for two reasons: (1) because the quality of the data, and the number of observed parameters, do not suppport inclusion of individual displacement parameters; (2) constraints on displacement parameters eliminate strong correlations with refined site scattering. The occupancy of all Mn, Cu and La sites were refined to gain information on the distribution of light elements such as Al and Mg. Atomic coordinates are given in Table 3, and selected interatomic distances are summarized in Table 4. Because only very few small crystals of stavelotite-(La) were found, so that no Gandolfi camera investigation was feasible, the X-ray powder pattern (Table 5) was calculated from the atomic coordinates for Debye-Scherrer geometry and Cu$K\alpha_1$ X-radiation using the program LAZY PULVERIX (Yvon *et al.*, 1977). It is believed that such calculated powder pattern is far superior to a weak Gandolfi pattern as the result of insufficient material.

Several problems became obvious before structure solution: (1) The structure exhibits strong pseudosymmetry

Table 3. Atomic coordinates, coordination, refined cation electron density (e/Å^3) and U_{iso} of stavelotite-(La).

Coord.	site	e/Å^3	x	y	z	U_{iso}
8	La(1)	55.7(4)	0.5668(2)	0.7852(3)	0.1895(1)	0.0112(2)
8	La(2)	55.7(4)	0.2129(3)	0.1087(3)	0.1898(1)	0.0112(2)
8	La(3)	55.7(4)	0.8894(3)	0.4356(3)	0.1894(1)	0.0112(2)
6	Mn(1)	25	0.5579(6)	0.9520(6)	0.2772(2)	0.0078(3)
6	Mn(2)	25	0.3631(6)	0.1101(6)	0.2791(2)	0.0078(3)
6	Mn(3)	25	0.4145(6)	0.6357(6)	0.2790(2)	0.0078(3)
6	Mn(4)	25	0.7339(6)	0.7774(7)	0.2790(2)	0.0078(3)
6	Mn(5)	22.5(4)	0.0435(7)	0.9326(7)	0.2788(2)	0.0078(3)
6	Mn(6)	25	0.2218(7)	0.2860(7)	0.2769(2)	0.0078(3)
6	Mn(7)	25	0.7150(6)	0.2654(6)	0.2784(2)	0.0078(3)
6	Mn(8)	25	0.0633(6)	0.4400(6)	0.2783(2)	0.0078(3)
6	Mn(9)	25	0.8885(6)	0.5852(5)	0.2782(2)	0.0078(3)
4+1	Mn(10)	25	0.2175(6)	0.2707(6)	0.0236(2)	0.0078(3)
5+1	Mn(11)	25	0.0504(6)	0.4387(6)	0.0189(2)	0.0078(3)
8	Mn(12)	23.8(4)	0.5541(7)	0.4450(8)	0.0243(2)	0.0078(3)
8	Mn(13)	25	0.2200(6)	0.7710(6)	0.0239(2)	0.0078(3)
8	Mn(14)	22.3(4)	0.8795(6)	0.1082(7)	0.0239(3)	0.0078(3)
4+1	Mn(15)	25	0.3862(6)	0.2806(6)	0.3531(2)	0.0078(3)
4+1	Mn(16)	25	0.2165(6)	0.9420(6)	0.3515(2)	0.0078(3)
4+2	Mn(17)	25	0.7188(6)	0.4335(6)	0.3547(2)	0.0078(3)
4+1	Mn(18)	25	0.8939(7)	0.2765(7)	0.3558(2)	0.0078(3)
4+2	Mn(19)	25	0.3958(7)	0.7877(6)	0.3552(2)	0.0078(3)
4+2	Mn(20)	25	0.0600(6)	0.6086(7)	0.3531(2)	0.0078(3)
4	Cu(21)	24.3(4)	0.0565(7)	0.1111(8)	0.3580(2)	0.0078(3)
6	Mn(22)	20.8(4)	0.3755(7)	0.2641(7)	0.1013(2)	0.0078(3)
6	Mn(23)	21.4(4)	0.7232(7)	0.9443(7)	0.0996(2)	0.0078(3)
6	Mn(24)	21.2(4)	0.0564(7)	0.6108(7)	0.0999(2)	0.0078(3)
6	Mn(25)	21.2(4)	0.2188(7)	0.9370(7)	0.1020(2)	0.0078(3)
6	Mn(26)	20.7(4)	0.5569(8)	0.6064(7)	0.1006(2)	0.0078(3)
6	Mn(27)	19.5(4)	0.7165(8)	0.4427(8)	0.1001(2)	0.0078(3)
6	Mn(28)	19.0(4)	0.3988(8)	0.7746(8)	0.0997(2)	0.0078(3)
6	Mn(29)	19.7(4)	0.0484(8)	0.1053(8)	0.1014(2)	0.0078(3)
6	Mn(30)	19.5(4)	0.8853(8)	0.2852(7)	0.0987(2)	0.0078(3)
	Si(1)		0.2378(10)	0.4605(10)	0.2060(3)	0.0084(5)
	Si(2)		0.5482(11)	0.4339(10)	0.1719(3)	0.0084(5)
	Si(3)		0.5379(9)	0.1097(11)	0.2069(3)	0.0084(5)
	Si(4)		0.2247(11)	0.7697(10)	0.1720(3)	0.0084(5)
	Si(5)		0.8871(10)	0.7588(9)	0.2065(3)	0.0084(5)
	Si(6)		0.8855(11)	0.1100(10)	0.1716(3)	0.0084(5)
	Si(7)		0.2228(13)	0.7759(13)	0.2683(3)	0.0084(5)
	Si(8)		0.5553(13)	0.4453(12)	0.2681(3)	0.0084(5)
	Si(9)		-0.1084(13)	0.1100(13)	0.2682(4)	0.0084(5)
	Si(10)		0.5519(13)	0.1058(12)	0.1099(4)	0.0084(5)
	Si(11)		0.2232(14)	0.4442(13)	0.1108(4)	0.0084(5)
	Si(12)		0.8860(13)	0.7720(13)	0.1106(4)	0.0084(5)
	O(1)		0.229(3)	0.775(3)	0.2210(8)	0.0132(6)
	O(2)		0.890(3)	0.117(3)	0.2189(8)	0.0132(6)
	O(3)		0.538(2)	0.973(2)	0.2200(8)	0.0132(6)
	O(4)		0.100(3)	0.457(3)	0.2207(8)	0.0132(6)
	O(5)		0.374(2)	0.596(3)	0.2225(8)	0.0132(6)
	O(6)		0.024(2)	0.892(2)	0.2213(8)	0.0132(6)
	O(7)		0.555(3)	0.634(3)	0.0397(8)	0.0132(6)
	O(8)		0.081(3)	0.108(3)	0.0443(8)	0.0132(6)
	O(9)		0.358(3)	0.246(3)	0.0471(8)	0.0132(6)
	O(10)		0.035(3)	0.587(3)	0.0415(8)	0.0132(6)
	O(11)		0.544(3)	0.429(3)	0.0878(7)	0.0132(6)
	O(12)		0.882(3)	0.306(3)	0.0387(8)	0.0132(6)
	O(13)		0.249(2)	0.476(2)	0.2917(8)	0.0132(6)
	O(14)		0.033(3)	0.253(3)	0.3797(8)	0.0132(6)
	O(15)		0.555(3)	0.299(3)	0.3741(8)	0.0132(6)
	O(16)		0.085(2)	0.435(2)	0.0922(8)	0.0132(6)
	O(17)		0.230(3)	0.643(3)	0.3738(8)	0.0132(6)

(to be continued)

Table 3 (continued)

site	x	y	z	U_{iso}
O(18)	0.570(2)	-0.009(2)	0.0938(8)	0.0132(6)
O(19)	0.343(2)	0.554(2)	0.0896(7)	0.0132(6)
O(20)	0.425(3)	0.098(2)	0.0909(7)	0.0132(6)
O(21)	0.667(2)	0.225(2)	0.0912(8)	0.0132(6)
O(22)	0.224(2)	0.313(2)	0.0961(8)	0.0132(6)
O(23)	0.536(2)	0.105(3)	0.1584(8)	0.0132(6)
O(24)	0.884(3)	0.761(2)	0.1582(9)	0.0132(6)
O(25)	0.361(3)	0.780(3)	0.1554(8)	0.0132(6)
O(26)	0.084(2)	0.639(3)	0.1538(8)	0.0132(6)
O(27)	0.414(3)	0.299(3)	0.1552(8)	0.0132(6)
O(28)	0.020(3)	0.115(2)	0.1570(8)	0.0132(6)
O(29)	0.225(3)	0.448(3)	0.1589(8)	0.0132(6)
O(30)	0.572(2)	0.776(3)	0.1121(7)	0.0132(6)
O(31)	0.205(2)	0.093(2)	0.1161(8)	0.0132(6)
O(32)	-0.120(3)	0.444(3)	0.1141(7)	0.0132(6)
O(33)	-0.114(3)	0.111(3)	0.0876(7)	0.0132(6)
O(34)	0.693(3)	0.922(3)	0.0412(8)	0.0132(6)
O(35)	0.015(2)	0.781(2)	0.0905(7)	0.0132(6)
O(36)	0.863(2)	0.895(2)	0.0956(7)	0.0132(6)
O(37)	0.749(2)	0.633(2)	0.0977(7)	0.0132(6)
O(38)	0.012(2)	0.224(2)	0.2873(7)	0.0132(6)
O(39)	0.886(2)	0.745(2)	0.2920(8)	0.0132(6)
O(40)	0.070(3)	0.969(3)	0.3360(8)	0.0132(6)
O(41)	0.431(3)	0.654(2)	0.3387(8)	0.0132(6)
O(42)	0.213(3)	0.254(3)	0.3373(8)	0.0132(6)
O(43)	0.346(3)	0.110(3)	0.3350(8)	0.0132(6)
O(44)	0.031(3)	0.435(3)	0.3358(8)	0.0132(6)
O(45)	0.890(3)	0.566(2)	0.3375(8)	0.0132(6)
O(46)	0.567(3)	0.927(3)	0.3379(8)	0.0132(6)
O(47)	0.523(2)	0.111(2)	0.2895(8)	0.0132(6)
O(48)	0.704(3)	0.786(3)	0.3363(8)	0.0132(6)
O(49)	0.748(3)	0.289(3)	0.3363(8)	0.0132(6)
O(50)	0.679(3)	0.436(2)	0.1554(8)	0.0132(6)
O(51)	0.672(2)	0.247(3)	0.2198(8)	0.0132(6)
O(52)	0.235(2)	0.323(3)	0.2201(8)	0.0132(6)
O(53)	0.558(3)	0.440(3)	0.2217(8)	0.0132(6)
O(54)	0.550(2)	0.570(2)	0.1556(8)	0.0132(6)
O(55)	0.885(2)	0.249(2)	0.1570(8)	0.0132(6)
O(56)	0.756(2)	0.980(2)	0.1529(7)	0.0132(6)
O(57)	0.224(3)	0.774(3)	0.0872(7)	0.0132(6)
O(58)	0.676(2)	0.428(2)	0.2869(8)	0.0132(6)
O(59)	0.221(2)	0.913(2)	0.2855(8)	0.0132(6)
O(60)	0.416(2)	0.313(2)	0.2851(8)	0.0132(6)
O(61)	0.225(3)	0.909(3)	0.1572(8)	0.0132(6)
O(62)	-0.127(2)	0.964(2)	0.2839(7)	0.0132(6)
O(63)	0.760(2)	0.113(2)	0.2834(7)	0.0132(6)
O(64)	0.591(2)	0.814(2)	0.2655(8)	0.0132(6)
O(65)	0.886(2)	0.409(2)	0.2638(8)	0.0132(6)
O(66)	0.755(3)	0.761(2)	0.2235(8)	0.0132(6)
O(67)	0.408(3)	0.109(3)	0.2226(8)	0.0132(6)
O(68)	0.189(2)	0.112(2)	0.2656(8)	0.0132(6)
O(69)	0.358(2)	0.779(2)	0.2852(7)	0.0132(6)
O(70)	0.572(2)	0.583(2)	0.2880(8)	0.0132(6)
O(71)	0.882(2)	0.622(2)	0.2219(8)	0.0132(6)
O(72)	0.094(2)	0.636(2)	0.2879(8)	0.0132(6)

of a rhombohedral lattice with a = 6.654, c = 33.347 Å (in hexagonal setting) caused by the distribution of the heavily scattering cations. As a consequence the diffraction pattern is characterized by few very strong reflections and a majority of reflections with very low intensity. The relation between the real (primitive trigonal) a axis and the pseudo

Table 4. Selected interatomic distances [Å] in stavelotite-(La).

La(1)-O(5)	2.46(3)	Mn(7)-O(58)	2.15(2)
La(1)-O(56)	2.52(3)	Mn(8)-O(44)	1.95(3)
La(1)-O(3)	2.55(3)	Mn(8)-O(65)	1.95(2)
La(1)-O(64)	2.55(3)	Mn(8)-O(4)	1.96(3)
La(1)-O(66)	2.58(3)	Mn(8)-O(13)	2.01(2)
La(1)-O(30)	2.59(3)	Mn(8)-O(72)	2.13(2)
La(1)-O(25)	2.60(3)	Mn(8)-O(38)	2.27(2)
La(1)-O(54)	2.64(3)	Mn(9)-O(39)	1.92(2)
La(2)-O(31)	2.46(3)	Mn(9)-O(71)	1.93(3)
La(2)-O(67)	2.49(3)	Mn(9)-O(45)	1.99(3)
La(2)-O(28)	2.51(3)	Mn(9)-O(65)	2.07(2)
La(2)-O(27)	2.54(3)	Mn(9)-O(72)	2.16(2)
La(2)-O(68)	2.55(3)	Mn(9)-O(58)	2.22(2)
La(2)-O(52)	2.56(3)	Mn(10)-O(48)	1.85(3)
La(2)-O(6)	2.58(3)	Mn(10)-O(46)	1.87(3)
La(2)-O(61)	2.61(3)	Mn(10)-O(8)	1.88(3)
La(3)-O(55)	2.39(3)	Mn(10)-O(9)	1.94(3)
La(3)-O(71)	2.44(2)	Mn(10)-O(22)	2.46(3)
La(3)-O(65)	2.50(3)	Mn(11)-O(41)	1.85(3)
La(3)-O(32)	2.52(2)	Mn(11)-O(12)	1.89(3)
La(3)-O(4)	2.54(3)	Mn(11)-O(48)	1.93(3)
La(3)-O(51)	2.57(3)	Mn(11)-O(10)	1.95(3)
La(3)-O(26)	2.58(3)	Mn(11)-O(70)	2.18(3)
La(3)-O(50)	2.68(3)	Mn(11)-O(16)	2.48(3)
Mn(1)-O(64)	1.85(2)	Mn(12)-O(11)	2.12(3)
Mn(1)-O(3)	1.95(3)	Mn(12)-O(7)	2.24(3)
Mn(1)-O(46)	2.05(3)	Mn(12)-O(15)	2.26(3)
Mn(1)-O(47)	2.10(2)	Mn(12)-O(49)	2.27(3)
Mn(1)-O(63)	2.14(2)	Mn(12)-O(46)	2.27(3)
Mn(1)-O(69)	2.18(3)	Mn(12)-O(47)	2.30(3)
Mn(2)-O(47)	1.87(2)	Mn(12)-O(9)	2.40(3)
Mn(2)-O(43)	1.87(3)	Mn(12)-O(43)	2.53(3)
Mn(2)-O(67)	1.95(3)	Mn(13)-O(57)	2.11(2)
Mn(2)-O(59)	2.04(3)	Mn(13)-O(13)	2.20(3)
Mn(2)-O(68)	2.07(2)	Mn(13)-O(10)	2.21(3)
Mn(2)-O(60)	2.11(3)	Mn(13)-O(42)	2.26(3)
Mn(3)-O(13)	1.92(2)	Mn(13)-O(17)	2.30(3)
Mn(3)-O(5)	1.94(3)	Mn(13)-O(44)	2.32(3)
Mn(3)-O(41)	2.00(3)	Mn(13)-O(14)	2.38(3)
Mn(3)-O(69)	2.06(2)	Mn(13)-O(41)	2.43(3)
Mn(3)-O(64)	2.10(2)	Mn(14)-O(33)	2.13(3)
Mn(3)-O(70)	2.20(2)	Mn(14)-O(39)	2.19(3)
Mn(4)-O(66)	1.89(3)	Mn(14)-O(34)	2.23(3)
Mn(4)-O(62)	1.94(2)	Mn(14)-O(40)	2.29(3)
Mn(4)-O(64)	1.94(2)	Mn(14)-O(12)	2.32(3)
Mn(4)-O(48)	1.95(3)	Mn(14)-O(48)	2.37(3)
Mn(4)-O(39)	2.01(2)	Mn(14)-O(8)	2.42(3)
Mn(4)-O(70)	2.10(2)	Mn(14)-O(45)	2.44(3)
Mn(5)-O(40)	1.94(3)	Mn(15)-O(43)	1.88(3)
Mn(5)-O(68)	1.95(3)	Mn(15)-O(42)	1.93(3)
Mn(5)-O(6)	1.96(3)	Mn(15)-O(10)	1.94(3)
Mn(5)-O(39)	2.06(2)	Mn(15)-O(15)	1.97(3)
Mn(5)-O(59)	2.18(3)	Mn(15)-O(60)	2.30(3)
Mn(5)-O(62)	2.18(2)	Mn(16)-O(43)	1.84(3)
Mn(6)-O(68)	1.89(3)	Mn(16)-O(40)	1.94(3)
Mn(6)-O(52)	1.93(3)	Mn(16)-O(34)	1.97(3)
Mn(6)-O(42)	2.04(3)	Mn(16)-O(7)	1.99(3)
Mn(6)-O(13)	2.11(2)	Mn(16)-O(59)	2.23(3)
Mn(6)-O(60)	2.11(2)	Mn(17)-O(15)	1.86(3)
Mn(6)-O(38)	2.18(2)	Mn(17)-O(45)	1.88(3)
Mn(7)-O(65)	1.90(3)	Mn(17)-O(12)	1.89(3)
Mn(7)-O(49)	1.96(3)	Mn(17)-O(49)	1.96(3)
Mn(7)-O(51)	2.00(3)	Mn(17)-O(58)	2.31(3)
Mn(7)-O(63)	2.07(2)	Mn(17)-O(21)	2.41(3)
Mn(7)-O(47)	2.07(3)	Mn(18)-O(44)	1.85(3)

(to be continued)

Table 4 (continued)

Mn(18)-O(49)	1.87(3)	Mn(28)-O(19)	2.31(2)
Mn(18)-O(14)	1.93(3)	Mn(29)-O(28)	1.89(3)
Mn(18)-O(9)	1.96(3)	Mn(29)-O(8)	1.94(3)
Mn(18)-O(20)	2.34(3)	Mn(29)-O(31)	1.94(3)
Mn(19)-O(7)	1.83(3)	Mn(29)-O(33)	1.96(3)
Mn(19)-O(41)	1.86(3)	Mn(29)-O(22)	2.24(3)
Mn(19)-O(17)	1.91(3)	Mn(29)-O(36)	2.30(2)
Mn(19)-O(46)	1.91(3)	Mn(30)-O(32)	1.93(3)
Mn(19)-O(19)	2.33(3)	Mn(30)-O(55)	1.99(3)
Mn(19)-O(69)	2.37(3)	Mn(30)-O(12)	2.02(3)
Mn(20)-O(45)	1.85(3)	Mn(30)-O(33)	2.05(3)
Mn(20)-O(34)	1.92(3)	Mn(30)-O(16)	2.09(3)
Mn(20)-O(17)	1.92(3)	Mn(30)-O(21)	2.26(2)
Mn(20)-O(44)	1.94(3)	Si(1)-O(29)	1.58(3)
Mn(20)-O(72)	2.20(3)	Si(1)-O(52)	1.64(3)
Mn(20)-O(18)	2.52(3)	Si(1)-O(4)	1.64(3)
Cu(21)-O(40)	1.86(3)	Si(1)-O(5)	1.67(3)
Cu(21)-O(42)	1.87(3)	Si(2)-O(50)	1.60(3)
Cu(21)-O(8)	1.88(3)	Si(2)-O(27)	1.64(3)
Cu(21)-O(14)	1.93(3)	Si(2)-O(54)	1.65(3)
Mn(22)-O(9)	1.82(3)	Si(2)-O(53)	1.66(3)
Mn(22)-O(27)	1.85(3)	Si(3)-O(67)	1.59(3)
Mn(22)-O(11)	1.97(3)	Si(3)-O(23)	1.62(3)
Mn(22)-O(31)	2.03(3)	Si(3)-O(51)	1.62(3)
Mn(22)-O(22)	2.09(3)	Si(3)-O(3)	1.64(3)
Mn(22)-O(20)	2.28(2)	Si(4)-O(25)	1.62(3)
Mn(23)-O(56)	1.82(3)	Si(4)-O(1)	1.63(3)
Mn(23)-O(30)	1.90(3)	Si(4)-O(61)	1.68(3)
Mn(23)-O(33)	1.94(3)	Si(4)-O(26)	1.68(3)
Mn(23)-O(36)	1.97(2)	Si(5)-O(24)	1.61(3)
Mn(23)-O(34)	1.97(3)	Si(5)-O(6)	1.63(3)
Mn(23)-O(18)	2.09(3)	Si(5)-O(71)	1.64(3)
Mn(24)-O(26)	1.83(3)	Si(5)-O(66)	1.64(3)
Mn(24)-O(57)	1.96(3)	Si(6)-O(2)	1.58(3)
Mn(24)-O(10)	1.96(3)	Si(6)-O(28)	1.60(3)
Mn(24)-O(32)	2.03(3)	Si(6)-O(56)	1.62(3)
Mn(24)-O(16)	2.23(2)	Si(6)-O(55)	1.67(3)
Mn(24)-O(35)	2.26(2)	Si(7)-O(1)	1.58(3)
Mn(25)-O(61)	1.87(3)	Si(7)-O(69)	1.64(3)
Mn(25)-O(14)	1.88(3)	Si(7)-O(72)	1.69(3)
Mn(25)-O(31)	1.94(3)	Si(7)-O(59)	1.69(3)
Mn(25)-O(57)	1.97(3)	Si(8)-O(53)	1.55(3)
Mn(25)-O(35)	2.16(2)	Si(8)-O(58)	1.63(3)
Mn(25)-O(20)	2.20(3)	Si(8)-O(70)	1.64(3)
Mn(26)-O(54)	1.87(3)	Si(8)-O(60)	1.67(3)
Mn(26)-O(30)	1.91(3)	Si(9)-O(38)	1.50(3)
Mn(26)-O(11)	2.02(3)	Si(9)-O(63)	1.62(3)
Mn(26)-O(7)	2.06(3)	Si(9)-O(2)	1.65(3)
Mn(26)-O(37)	2.08(2)	Si(9)-O(62)	1.67(3)
Mn(26)-O(19)	2.26(2)	Si(10)-O(21)	1.49(3)
Mn(27)-O(50)	1.89(3)	Si(10)-O(18)	1.54(3)
Mn(27)-O(32)	1.94(3)	Si(10)-O(20)	1.56(3)
Mn(27)-O(11)	1.96(3)	Si(10)-O(23)	1.63(3)
Mn(27)-O(15)	2.00(3)	Si(11)-O(19)	1.50(3)
Mn(27)-O(37)	2.03(2)	Si(11)-O(22)	1.59(3)
Mn(27)-O(21)	2.30(2)	Si(11)-O(29)	1.60(3)
Mn(28)-O(25)	1.92(3)	Si(11)-O(16)	1.66(3)
Mn(28)-O(17)	1.99(3)	Si(12)-O(35)	1.59(3)
Mn(28)-O(30)	2.03(3)	Si(12)-O(24)	1.59(3)
Mn(28)-O(57)	2.05(3)	Si(12)-O(36)	1.64(3)
Mn(28)-O(18)	2.29(3)	Si(12)-O(37)	1.65(3)

Table 5. X-ray powder pattern for stavelotite-(La) calculated from refined atomic coordinates (program Lazypulverix (Yvon *et al.*, 1977)) for Cu$K\alpha_1$ radiation and Debye-Scherrer geometry. The d-values of the 12 strongest lines are underlined.

h	*k*	*l*	d	I/I_0
0	0	3	11.116	18
1	1	1	5.678	3
1	1	-2	5.446	31
1	1	-5	4.360	5
1	1	7	3.6716	5
1	1	-8	3.3774	7
3	0	0	3.3270	12
0	3	3	3.1873	19
3	0	3	3.1873	19
2	2	-1	2.8706	6
3	0	6	2.8546	7
0	3	6	2.8546	7
2	2	2	2.8302	5
0	0	12	2.7789	40
2	2	-4	2.7232	100
1	1	-11	2.6829	8
2	2	5	2.6450	1
3	0	9	2.4755	3
0	3	9	2.4755	3
2	2	-7	2.4654	2
2	2	8	2.3702	29
1	1	13	2.3435	2
0	0	15	2.2231	8
1	1	-14	2.2013	12
4	1	-2	2.1597	9
1	4	-2	2.1597	9
0	3	12	2.1328	1
3	0	12	2.1328	1
1	4	7	1.9808	1
4	1	7	1.9808	1
3	3	3	1.8928	3
3	3	-3	1.8928	4
0	3	15	1.8484	2
3	0	15	1.8484	2
4	1	10	1.8235	1
1	4	10	1.8235	1
3	3	6	1.8155	5
1	4	-11	1.7688	2
4	1	-11	1.7688	2
3	3	9	1.7053	1
2	2	-16	1.6887	28
1	1	19	1.6790	2
6	0	0	1.6635	40
2	2	17	1.6215	1
4	1	-14	1.6074	2
1	4	-14	1.6074	2
3	3	12	1.5801	1
2	2	-19	1.4989	4
3	3	-15	1.4535	2
2	2	20	1.4431	13
0	6	12	1.4273	10
6	0	12	1.4273	10
4	4	4	1.4196	9
2	5	11	1.4138	1
5	2	11	1.4138	1
1	1	-23	1.4060	2
0	0	24	1.3895	1

a axis is: $a_{real} = a_{pseudo} \times \sqrt{3}$. (2) A **c**-axis length of 33.347 Å for a primitive lattice leads to closely spaced diffraction spots in reciprocal space, which cannot be completely separated during intensity integration. In other words, the flanks

of strong reflections are leaking into adjacent diffraction spots. This effect is particularly critical in stavelotite because of the low intensity of many reflections. These weak reflections 'inherit' false intensity due to the 'leaking' from adjacent strong diffractions. As a compromise we have chosen a relatively short exposure time for frame collection in order to keep the size of the diffraction spots from strong reflections controllable. The disadvantage of this approach is the large number of reflections with $F_{obs} < 4\sigma$ (F_{obs}) of *ca*. 70 %. Careful analyses of reflection profiles and check of symmetry related reflections indicated that the space group of stavelotite is either *P*3-(#147), *P*3 (#143), $P3_1$ (144), $P3_2$ (#145), *P*31*m* (#157), *P*3-1*m* (#162), *P*312 (#149), $P3_112$ (#151), or $P3_212$ (#153). Subsequent structure solutions were attempted in the former three first space groups yielding only successful structure solution in $P3_1$. Subsequent tests for higher symmetry indicated that $P3_1$ is indeed the correct space group. The high value of R_σ = 13.3 % (counting statistics) is a consequence of the large number of weak reflections. Considering the problems stated above it is not surprising that the final R_1 value converged only at 10 %. Nevertheless, the structure of stavelotite-(La), comprising 117 symmetry independent atomic sites (72 O, 12 Si, 3 La, and 30 transition-metal positions), is well defined without any unusual features from a crystal chemical point of view. For acentric structures, such as space group $P3_1$, the SHELXTL program package calculates the so called Flack parameter indicating whether the absolute structure can be determined and whether twinning by the inversion operation must be assumed. In case of the investigated stavelotite-(La) crystal twinning was suggested; thus in the final refinement theTWIN option was activated converging at 0.46(7):0.54(7) twin portions.

The densely packed structure can best be explained by dividing it into four polyhedral layers stacked parallel to **c** (Fig. 3).

Layer 1, centered by cations at z = 0.02 and z = 0.02 + 1/3 (Mn(10) to Cu(21)), is characterized by eight-coordinated (distorted cubes) Mn^{2+} sites connected by edge-sharing with strongly distorted Mn^{3+} polyhedra. The polyhedra around Mn^{3+} resemble either elongated tetragonal bipyramids or tetragonal pyramids where the pyramidal apex is elongated. Such coordinations are characteristic for d^4 Jahn-Teller cations such as Mn^{3+} (Moore *et al.*, 1991; Hoffmann *et al*., 1997). In addition, one site Cu(21) has a planar square coordination with an average Cu(21)-O distance of 1.889 Å which is typical for Jahn-Teller active Cu^{2+} (Burns & Hawthorne, 1995; Starova *et al*., 1998). The next closest O sites around Cu(21) are 2.77 Å (O(35)) and 2.86 Å (O(38)) apart. At least in silicates and oxides we are not aware of other cations (except Cu) found in stavelotite which would select nearly planar four-fold coordination. Several electron-microprobe analyses of stavelotite show less than 1 Cu pfu suggesting that, if not enough Cu is available, the Cu(21) coordination becomes either five or six-coordinated (*e.g*. suitable for Mn^{3+}). This should lead to smearing of the central site or/and the oxygen apices. However, because only

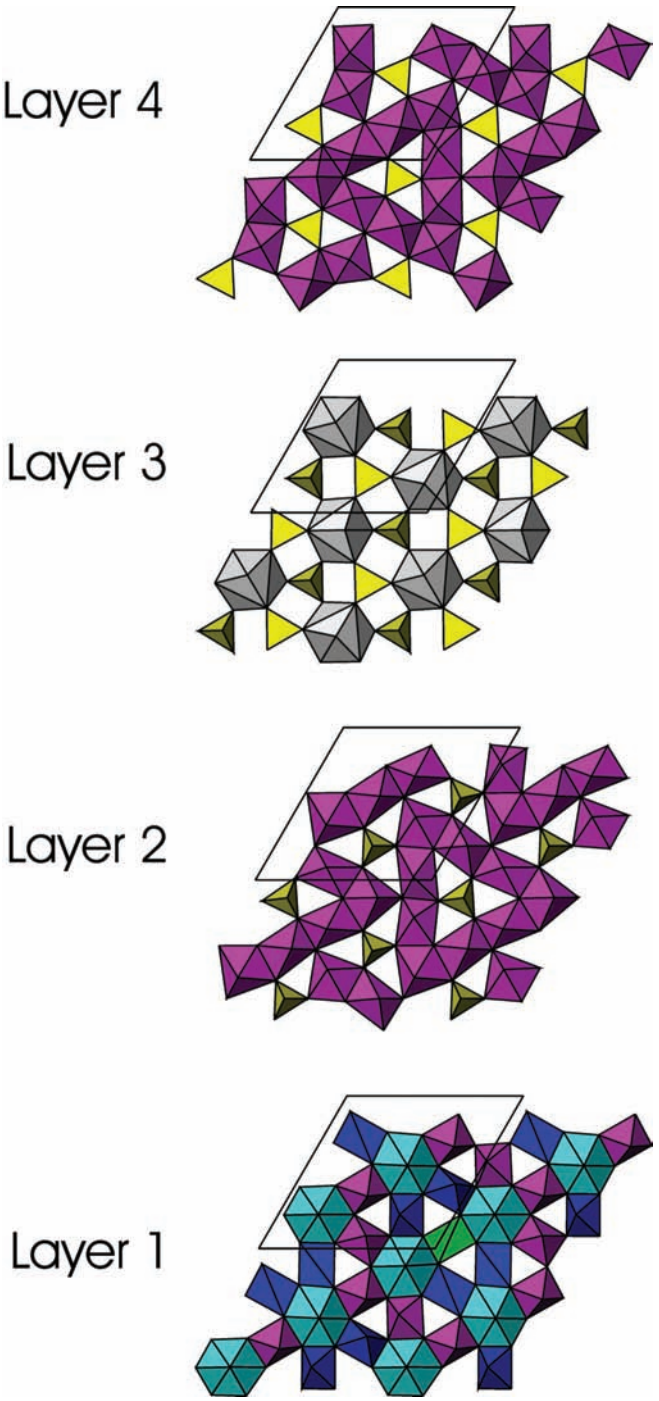

Fig. 3. Polyhedral layers in stavelotite. Layer 1 is formed by cubes (light blue) of eight-coordinated Mn^{2+}. Magenta octahedra (strongly elongated to tetragonal bipyramids) and violet tetragonal pyramids are centered by mainly Mn^{3+}. Cu^{2+} (green) possesses square planar coordination. Layer 2 of Mn_9Si_3 composition is formed by edge- and corner sharing Mn^{3+} octahedra (magenta) where tetrahedral Si (yellow) occupies trigonal interstices. All tetrahedral apices have the same orientation. Layer 3 of REE_3Si_6 composition is formed by grey cubes centered by REE connected in a pinwheel-like fashion by SiO_4 tetrahedra (yellow). 50 % of the tetrahedral apices are oriented up und 50 % are oriented down. Layer 4 is an inverted variety of layer 2.

average isotropic displacement parameters were refined in the present study we have no indication for such behaviour.

Layer 2, centered by cations at z = 0.10 and z = 0.10 + 1/3 (Mn(22)-Mn(30), Si(10)- Si(12)) is composed of Mn octahedra and Si tetrahedra. The octahedra are more regular than those in layer 1 and exhibit in general a lower electron density than 25 e/Å^3 (Mn) indicative of a mixed occupancy by major Mn with additional Al, Sc, and Mg. In addition to Mn^{3+}, tetravalent Mn necessary for charge balance may be disordered over such octahedra. SiO_4 tetrahedra in this layer are hosted at trigonal gaps formed by the arrangement of octahedra. All tetrahedra have the apex oriented in the same direction (upwards). Because there are three tetrahedra and nine octahedra in this layer it may be named T_3M_9 layer.

Layer 3 is formed by REE in eight-fold coordination (cubes) at z = 0.19 and z = 0.19 + 1/3 ((La(1)-La(3)) edge-connected by SiO_4 tetrahedra ((Si(1)-Si(6)) where three tetrahedra have the apex up and three the apex down.

Layer 4 is similar to layer 2 but the tetrahedra are inverted (apex downwards). Layer 4, also of T_3M_9 composition, is centered by Mn(1)-Mn(9) at z = 0.29 and z = 0.29 + 1/3 and Si(7)-Si(9). The electron density at all Mn sites within this layer is close to 25 e/Å^3 thus mainly Mn^{3+} and Mn^{4+} must be assigned.

If we consider layer 3 as central layer, layers 2 and 4 are attached above and below in a way that units of Si_2O_7 (disilicate) are formed. Two topological types of Si_2O_7 entities exist: those (4 ×) where the upper and lower tetrahedral base match each other and those (2 ×) where the triangular bases are rotated 60° against each other. All disilicate groups have rather stretched Si-O-Si angles between 173 and 177°. The O sites linking two tetrahedra are on general positions and are not bonded to other cations. It is assumed that the unusual Si-O-Si angles are a consequence of the dense arrangement of anions and cations in the stavelotite structure.

A qualitative check of oxygen bond-strengths indicates that all O sites have bond-strengths values close to 2, so that hydroxylation in stavelotite-(La) seems unlikely. Moreover, all O sites within the structure, which are not coordinated to Si, have distorted tetrahedral coordination by cations. Thus there is not even space for potential hydroxylation. O sites linking two SiO_4 tetrahedra cannot be hydroxylated because of bond valence arguments. The same also holds for O sites forming one tetrahedral apex with additional bonds to Mn and La. Thus the stavelotite-(La) crystal structure clearly suggests it to be an anhydrous mineral.

If we consider 1 Cu pfu (planar four-fold coordinated site Cu(21)) as essential for the investigated stavelotite-(La), a simplified charge-balanced formula may be written as La^{3+}_3 Mn^{2+}_3 Cu^{2+} $(Mn^{3+}_{25}Mn^{4+})_{\Sigma=26}$ $(Si_2O_7)_6O_{30}$, Z = 3. Any Ca substituting for REE^{3+}, and Mg, Co^{2+} as well as excess Cu^{2+} > 1.0 substituting for Mn^{3+} increase Mn^{4+} correspondingly.

Stavelotite-(La) belongs to a series of modular structures where single layers comprising different polyhedral arrangements are assembled to stacks (Fig. 4). All of the layers found in stavelotite-(La) have been described before (though in a slightly modified way) for other structures.

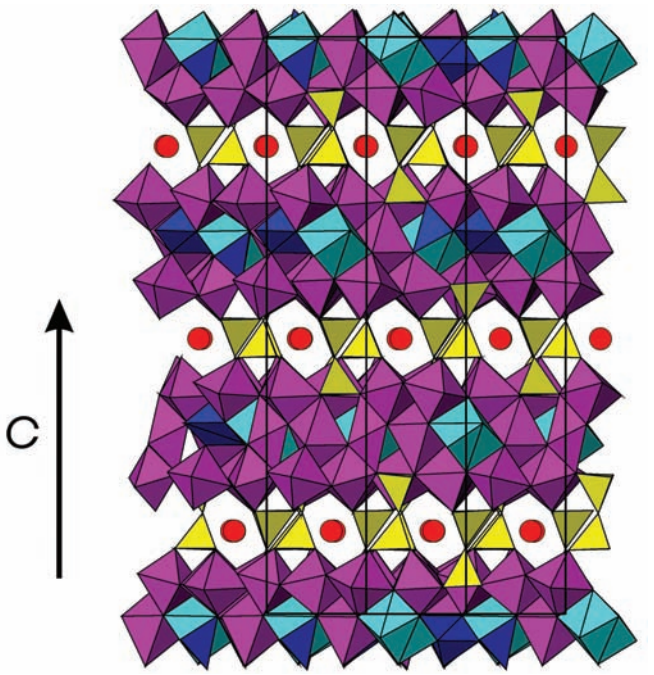

Fig. 4. Stacking of layers in stavelotite parallel to **c**. For color codes see Fig. 3. For clarity, REE in layer 3 are not drawn as cubes but as red spheres. Note the staggered Si_2O_7 units between layers 2 and 4.

Layer 1 has almost its exact counterpart in långbanite (Moore *et al*., 1991; Giuseppetti *et al*., 1991) and the same arrangement of octahedra also occurs in pyrochlore and the alunite-jarosite family. Layers 2 and 4 are also observed in långbanite (Moore *et al*., 1991) and are considered mitridatite-like. Layer 3, pinwheels linked to layers, is known as glaserite layer (for a review see Hawthorne *et al*., 2000). In glaserite $K_3Na(SO_4)_2$ the pinwheels are not centered by cubes arranged parallel (111) but by NaO_6 octahedra.

Moore *et al.* (1991) derived the långbanite structure from closest packing of cations. This is only partly true for stavelotite (Fig. 5). There is a sequence of three closest-packed cation layers (ABC) interrupted by the glaserite-like layer. The glaserite-like cation layer also displays close packing of REE and Si. However, this packing is not commensurate with the packing of the two adjacent layers because the nearest cation-neighbour distance in the glaserite-like layer is *ca*. 3.9 Å whereas the corresponding distance in the adjacent layers is *ca.* 3.4 Å. Another description of the same observation is that layers 1, 2, and 4 are formed by 12 cations whereas layer 3 (glaserite-like) is only built by 9 cations.

Chemical composition and structural formula

Electron microprobe analyses on stavelotite-(La) were performed in the section Cor 8-2 using the CAMECA SX 50 instrument available at the Ruhr-Universität Bochum, with 20 kV acceleration voltage and 20 nA beam current. The beam

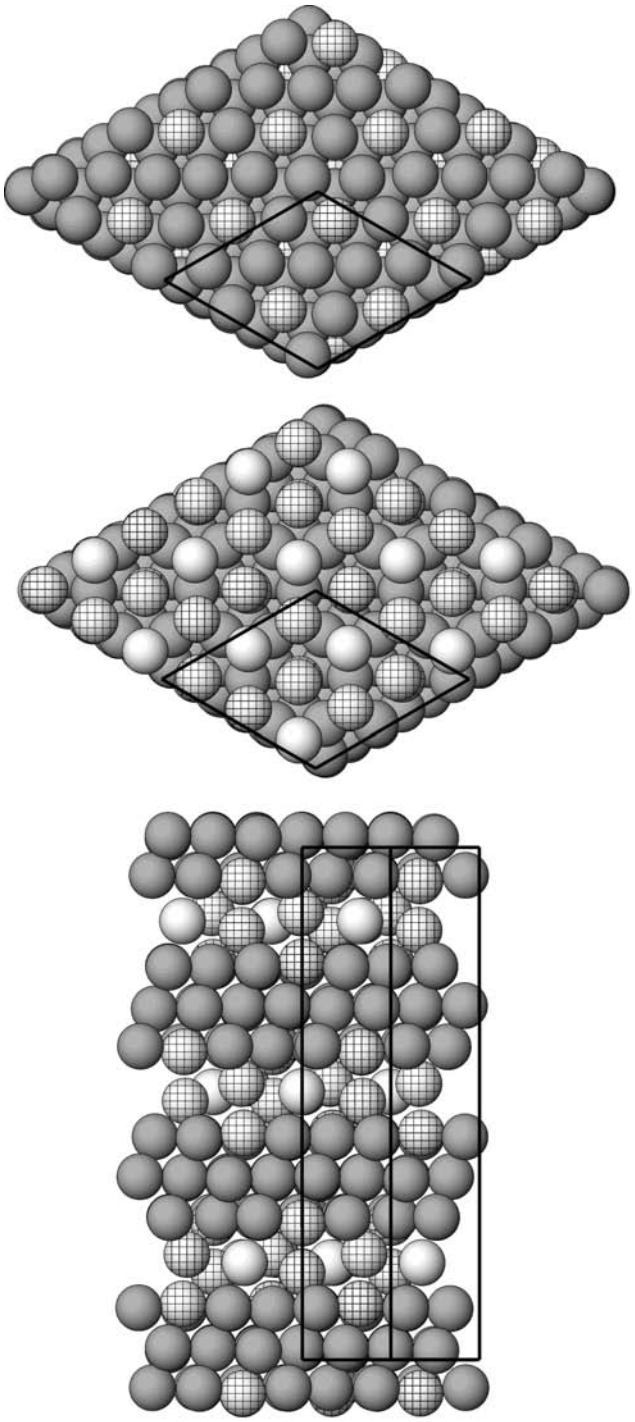

Fig. 5. Closest cation packing in stavelotite. Top: Close packed cation arrangement in layers 2 and 4 of Si_3Mn_9 composition, Mn grey, Si hatched. Middle: Close packed cation arrangement in layer 3 of REE_3Si_6 composition, REE light, Si hatched. For discussion consult text. Bottom: Stacking sequence of cation layers parallel to **c**. The Mn (grey) dominant layers have ABC stacking sequence which is disturbed by intercalation of REE_3Si_6 layers.

was focussed to about 1 µm. Standards employed were synthetic spessartine (Mn-*K*α), synthetic pyrope (Si-*K*α, Al-*K*α, Mg-*K*α), synthetic andradite (Fe-*K*α, Ca-*K*α), synthetic rutile (Ti-*K*α), synthetic cuprite (Cu-*K*α), synthetic silicate glasses (La-*L*α, Nd-*L*α, Ce-*L*α) and the following pure metals: Co (*K*α) Sc (*K*α). The analyses were corrected using the PAP procedure provided by CAMECA.

65 trustworthy analyses were performed in various portions of six distinct, partly polycrystalline masses of stavelotite-(La). These portions were chosen on account of their slightly different degrees of brightness in the BSE images of the irregularly zoned stavelotite crystals. Table 6 lists a selection of eight analyses, which includes most of the extreme element concentrations found in the crystals, arranged in the order of decreasing La contents. 13 cations were found in quantities that could be analyzed. Except for La and Nd, and in a few cases Mn, their concentrations do not vary widely. Most notable is the relative constancy of Si. The brighter areas in the BSE images turned out to be mainly due to slightly higher than average concentrations of Fe and Cu relative to the lighter element Mn. Surprizing is the appearance of the element scandium reaching as much as 4.21 wt.% Sc_2O_3. Copper is, according to the structure determination, an essential element of stavelotite-(La). Its maximum concentration of 3.73 wt.%, however, exceeds the amount necessary to fill the one site in the stavelotite structure nearly by a factor of two. The "traditional" elements Mg, Al, Ca and Ti, and surprizingly also Co, occur only in relatively small or minor quantities, whereas Fe is the third common element sharing structural positions with Mn^{3+}. Among the REE, only lanthanum and neodymium appear in major amounts, whereas cerium is always a minor element. La consistently dominates Nd, but in quite variable proportions, while the sum of the two is rather constant near 11-12 wt.% La_2O_3+Nd_2O_3. On an atomic basis, the La/Nd ratios vary between 1.3 and 5.2.

Somewhat disturbing are the low analytical totals near 97 wt%, which are hard to explain, because no other elements with atomic numbers greater than 6 could be detected. Higher valence states of Mn would raise the totals. Possibly, there are additional REE in concentrations too low to be detected individually, but their sums might count. There are no structural indications for hydroxylation (see previous section) nor for the presence of any molecular water. The good agreement of stoichiometry derived from both structural and analytical data (see below) supports the validity of the results. Nearly complete occupancy of all 45 cation positions (Table 6) leaves hardly any space for the presence of light elements like Li,Be and B.

It can also be pointed out that our optical measurements are consistent with the chemical data. Owing to the reflectance measurements, a mean index of refraction has been calculated as $n = 2.14 \pm 0.01$ (Table 1). With the calculated density, a K_p value can be deduced, according to the Gladstone-Dale relationship; this value is 0.254. By using the individual Gladstone-Dale constants, k_i, revised by Mandarino (1981), particularly the k_i of Mn_2O_3 (= 0.301) and of Fe_2O_3 (= 0.315), the K_c value of stavelotite-(La) becomes 0.246 when calculated with the mean chemical composition given in Table 6. These K_p and K_c values yield a compatibility index of -0.032 which ranges in the category "excellent" following Mandarino (1981).

The recalculations of cations per formula unit (pfu) in Table 6 is based on 72 oxygens and 45 cations. Iron is consid-

Table 6. Selected electron microprobe analyses of stavelotite-(La) and overall averages.

	61	17	30	43	32	56	4	68	Mean	Ranges	Ideal
SiO_2	19.88	20.43	20.19	20.24	20.11	20.47	20.27	20.08	20.17	19.79-20.72	20.20
TiO_2	0.42	0.60	0.39	0.43	0.32	0.46	0.45	0.48	0.44	0.31- 1.13	
MnO_2	5.53	5.18	6.17	5.00	4.66	6.24	4.21	4.49	4.83	2.62- 6.34	2.44
Mn_2O_3	27.87	30.17	26.13	32.46	32.62	27.47	33.29	38.47	31.67	26.13-38.47	39.81
MnO	5.90	6.00	6.03	6.02	5.99	6.09	6.04	5.97	5.99	5.86- 6.09	5.96
Al_2O_3	2.51	3.12	4.22	4.07	3.35	4.25	3.34	2.29	3.30	2.29- 4.25	
Fe_2O_3	14.72	12.95	12.14	11.04	13.18	11.76	13.64	13.52	13.08	11.04-15.93	15.66
Sc_2O_3	1.82	1.73	4.21	1.40	1.17	4.06	0.70	0.24	1.47	0.24- 4.21	
La_2O_3	10.25	9.58	9.04	8.90	8.32	8.08	7.49	5.91	8.39	5.91-10.25	13.69
Nd_2O_3	2.04	2.64	3.16	3.27	3.51	3.23	3.79	4.63	3.39	2.04- 4.63	
Ce_2O_3	1.26	0.63	0.28	0.26	0.16	0.28	0.32	0.57	0.44	0.16- 1.26	
CaO	0.29	0.39	0.45	0.25	0.29	0.49	0.32	0.44	0.33	0.20- 0.51	
MgO	0.83	0.98	0.77	1.18	1.18	0.81	1.18	0.66	1.06	0.66- 1.23	
CuO	3.29	2.70	3.73	2.15	1.67	3.67	1.32	0.70	2.11	0.70- 3.73	2.23
CoO	0.14	0.14	0.13	0.16	0.17	0.13	0.20	0.24	0.18	0.10- 0.24	
Σ	96.76	97.25	97.05	96.84	96.69	97.46	97.00	96.81	96.86	95.60-97.66	99.99
Atoms per formula unit (72 oxygen atoms, 45 cations) Large ions in eightfold coordination											
	61	17	30	43	32	56	4	68	Rec.M	(Ranges[1])	Ideal[2]
La	2.269	2.088	1.957	1.932	1.811	1.733	1.621	1.293	1.828		3.00
Nd	0.437	0.557	0.663	0.688	0.739	0.670	0.794	0.978	0.715		
Ce	0.277	0.137	0.060	0.056	0.035	0.061	0.068	0.125	0.095		
Ca	0.017	0.218	0.282	0.159	0.183	0.308	0.200	0.277	0.209		
Sc	--	--	0.038	0.165	0.231	0.228	0.317	0.124	0.153		
Σ_{large}	3.000	3.000	3.000	3.000	2.999	3.000	3.000	2.797	3.000		3.00
Manganese in eightfold (cube) coordination											
Mn^{2+}	2.999	3.001	2.997	2.998	2.997	2.998	3.003	2.998	2.998		3.00
R^{2+} in fourfold (square) coordination											
Cu	1.000	1.000	1.000	0.956	0.745	1.000	0.583	0.312	0.941		1.00
Mn^{3+}	--	--	--	0.044	0.255	--	0.417	0.688	0.058		
Σ_{square}	1.000	1.000	1,000	1.000	1.000	1.000	1.000	1.000	0.999		1.00
Cations in octahedral and five-coordinated positions											
Mn^{3+}	12.733	13.566	11.679	14.538	14.663	12.156	14.866	16.678	14.183		18.00
Fe^{3+}	6.649	5.756	5.362	4.888	5.859	5.146	6.019	6.035	5.814		7.00
Al	1.779	2.170	2.919	2.824	2.330	2.915	2.307	1.598	2.298		
Ti^{4+}	0.190	0.266	0.173	0.192	0.141	0.173	0.200	0.212	0.195		
Sc	0.951	0.891	2.118	0.553	0.370	1.829	0.040	--	0.604		
Ca	0.170	0.032	--	--	--	--	--	--	--		
Cu	0.491	0.203	0.654	--	--	0.609	--	--	--		
Mg	0.739	0.864	0.678	0.991	0.783	0.704	0.614	0.583	0.933		
Co	0.068	0.066	0.063	0.075	0.078	0.062	0.093	0.114	0.085		
Mn^{4+}	2.295	2.117	2.503	2.033	1.904	2.509	1.705	1.074	1.973		1.00
$\Sigma_{[5]+[6]}$	26.065	25.931	26.149	26.094	26.128	26.103	25.843	26.294	26.085		26.00
Tetrahedral cation											
Si	11.935	12.066	11.853	11.906	11.875	11.899	12.154	11.909	11.915		12.00

Eight individual analyses are labelled with their original laboratory numbers.
Mean = Mean concentrations of all 65 analyses.
Rec. M = Recalculation of mean analysis (independently of other recalculations).
Ranges involve all 65 anlyses.
[1] For the compositional ranges given, the atoms per formula unit were omitted because of uncertain site allocations of atoms.
[2] The idealized formula shown is modelled as discussed in the text assuming Mn^{3+}/Fe^{3+} = 18/7.

ered to be trivalent only. Manganese valences were initially distributed as required by the structural formula derived in the previous section:

$(REE)_3\ (Mn^{2+})_3\ Cu^{2+}\ (Mn^{3+}, Fe^{3+}, Mn^{4+})_{26}\ (Si_2O_7)_6\ O_{30}$.

Additional elements, modified manganese valences as well as excess amounts of elements relative to this formula were distributed in Table 6 as follows:

1. La, Nd and Ce were allocated to the eight-coordinated cube positions of REE in structural layer 3 (Fig. 3). Because their amounts are consistently below 3.0 pfu, Ca^{2+} was assigned to enter these positions on account of its similar ionic radius. However, quite often Ca does not suffice to fill the position up to 3.0 pfu, in which case the relatively large Sc^{3+} (in eightfold coordination) was allocated for the

rest. However, the main portion of Sc has to be attributed to other sites. For one analysis (no. 68), La+Nd+Ce+Ca+Sc is below 3.0 resulting in vacancies.

2. Of the total amount of Mn, 3.0 cations pfu are taken as Mn^{2+} to occupy the eightfold coordinated cubes of layer 1 (Fig. 3).
3. Cu^{2+} is allocated to the fourfold square position in layer 1, but is not always sufficient to fill it completely. In such cases, Mn^{3+} was tentatively used for the rest up to 1.0 pfu (see above). However, there are also cases with Cu in excess of 1.0 pfu; this excess was attributed to octahedral sites. Cu^{2+} like Ca introduces a charge deficiency, which is taken to be balanced here by equivalent amounts of Mn^{4+} in octahedral sites. Note that, with this procedure, stavelotite-(La) is considered to carry Mn in three different valence states.
4. The remaining Mn, all Fe^{3+}, Al, Ti, Mg and Co, as well as any rest amounts of Sc, Cu and Ca are assigned to the 26 octahedral and five-coordinated positions of layers 1, 2 and 4 (Fig. 3). The amounts of Mn^{4+} are calculated for charge balance to equal the sum of the divalent elements (Cu+Co+Mg+Ca), but minus Ti. The now remaining Mn is taken as Mn^{3+}, making up about one half of these structural positions.
5. The Si tetrahedra of layers 2-4 (Fig. 3) are assumed to be solely occupied by this element.

As a result, the structural formula derived from crystallographic work is rather well substantiated by the chemical variations determined (Table 6). The formula recalculated from the mean oxide weight percentages of the 65 analyses closely approaches the ideal formula. In detail, Si pfu fluctuates only slightly around its ideal value 12.0. With the cation allocation method described before, Si-variations must be correlated with similarly small deviations of the sums of octahedral plus five-coordinated atoms from 26.0. Nevertheless, we refrained from normalization to 12.0 Si atoms in order to confirm the impressive constancy of this element. A few analyses exhibit relatively strong variations of the most common element Mn, especially as Mn^{3+}, often with equivalent variations of Al and Sc for compensation (*e.g.* analysis no.30 of Table 6). The highest Mn^{3+} value (analysis no.68 of Table 6) was first suspected to be due to contamination by a Mn-oxide, because Al, Sc, La and Cu show minimum amounts. However, Si is normal and Nd at maximum, so that (La+Nd) is still quite normal. Therefore, analysis no.68 may yet represent a single-phase stavelotite-(La) with an unusual, extreme composition most strongly deviating from the mean composition of the 65 analyses (Table 6).

The most obvious chemical variation of the stavelotite-(La) crystals studied is undoubtedly their changing ratio of La *versus* Nd, which altogether show a good linear negative correlation.

Discussion

The new mineral stavelotite-(La) presents new facts, but also poses several questions relating both to its own existence and to its occurrence in the Le Coreux locality of manganese minerals. Some of them are enumerated here.

1. As mentioned before, the chemical composition of stavelotite-(La) is unique among silicates. The closest chemical similarity is to the new epidote-group mineral androsite-(La), which has less Mn, but Ca and Al as additional major components (Bonazzi *et al*., 1996). Thus, the appearance of these two minerals as accessory phases is probably restricted to highly oxidized Mn deposits, in which La and other REE occur as well. While for the growth of stavelotite-(La) a mobilization of both Mn and La by siliceous fluids was necessary, androsite-(La) occurs within the manganese ore itself (Bonazzi *et al*., 1996). It is noteworthy that the combination of REE with exceptionally high concentrations of manganese is also very rare in other than silicate minerals. The members of the retzian group, $Mn_2(Ce,La,Nd)$ $[(OH)_4AsO_4]$, are among these (Dunn & Sturman, 1982). The rarity of the combination of REE and Mn is somewhat surprizing as – geochemically speaking – REE are often enriched in manganese deposits, *e.g.* in marine manganese nodules (Fleet, 1984).

2. The occurrence of REE minerals in the Ottré Formation (Salm Group) is not unusual. Perhaps best known is the phosphate mineral florencite-Ce, $CeAl_3(PO_4)_2(OH)_6$ (*e.g.* Theunissen & Martin, 1969; Hanson, 1983). REE were also found as minor constituents in epidote-group minerals occurring in Mn deposits of the Stavelot Massif: Kramm (1979) analysed an unusual piemontite from Le Coreux containing 5.0 wt% of $(REE)_2O_3$, and Schreyer *et al.* (1986) found an allanite-like mineral containing about 9 wt% of $(REE)_2O_3$ in the Lienne valley. In these minerals either La or Ce are the dominant REE. The occasional rarity of Ce, as in stavelotite-(La), could possibly be caused by the high oxidation potentials prevailing in these manganese deposits, which may lead to the formation of tetravalent Ce with an ionic radius 15 % lower than of Ce^{3+}. The question remains open as to whether the dominance of La in stavelotite-(La) is due to a REE fractionation process during its growth, or due to the individual geochemical environment of the Le Coreux deposit.

3. For stavelotite-(La) the presence of Cu as an essential element stabilizing this mineral may represent another very important criterion for its growth at Le Coreux. Compared to braunite from the quartz veins of this same locality, which contains Cu as well (Schreyer *et al.*, 2001), Cu is enriched in stavelotite-(La) by up to one order of magnitude. In the structurally somewhat similar mineral långbanite, $(Mn^{2+},Ca)_4$ $(Mn^{3+},Fe^{3+})_9$ $Sb^{5+}[O_{16}/(SiO_4)_2]$, from a Swedish Mn-deposit the element antimony seems to play a stabilizing role as well.

4. The Mn-Si bearing fluids that formed the post-tectonic hydrothermal quartz veins at Le Coreux incorporated an interesting spectrum of trace elements that became minor or even major elements in the minerals deposited: Ba, Sr, Pb in hollandite-strontiomelane (Schreyer *et al*., 2001); Zn, Cu in braunite (loc.cit.); La, Nd, Ce, Sc, Cu and Co in stavelotite-(La) (this paper).

5. As to classification, stavelotite-(La) is a sorosilicate. Following Strunz & Nickel (2001) it may be grouped into

subdivision 9.BE (Si_2O_7 groups with additional anions; cations in octahedral [6] and greater coordination) compared to långbanite (formula see in 3.), which is a nesosilicate of subdivision 9.AG (with additional anions; cations in (mostly) [6] and >[6] coordination). The Si:O ratio of stavelotite-(La) (= 1:6) is twice that of långbanite (= 1:12).

Acknowledgements: We are very grateful to Olaf Medenbach, Bochum, who extracted the single crystal studied structurally from the thin section. Ernst Burke, Amsterdam, provided valuable hints prior to submission of the new mineral data to the IMA Commission. We appreciate the constructive journal reviews by Peter Burns and an anonymous referee.

References

Bonazzi, P., Menchetti, S., Reinecke, T. (1996): Solid solution between piemontite and androsite-(La), a new mineral of the epidote group from Andros Island, Greece. *Am. Mineral.*, **81**, 735-742.

Bruker AXS (1997): XPREP Ver. 5.1: A computer program for data preparation and reciprocal space exploration. Bruker Analytical X-ray systems, Madison, WI 53719-1173, USA .

— (1998): SHELXTL. 5.1/NT: A software package for structure solution and refinement. Bruker Analytical X-ray systems, Madison, WI 53719-1173, USA.

— (1999): SAINT+ Ver. 6.01/NT: A computer program for data reduction. Bruker Analytical X-ray systems, Madison, WI 53719-1173, USA .

Burns, P.C. & Hawthorne, F.C. (1995): Coordination-geometry structural pathways in Cu^{2+} oxysalt minerals. *Can. Mineral.*, **33**, 889-905.

Corin, F. (1968): Le défilé de la Salm entre Vielsalm et Salm-Château. *Bull. Soc. belge Géol.*, **77**, 155-174.

Dunn, P.J. & Sturman, B.D. (1982): Retzian-(Nd), a new mineral from Sterling Hill, New Jersey and a redefinition of retzian. *Am. Mineral.*, **67**, 841-845.

Fleet, A.J. (1984): Aqueous and sedimentary geochemistry of the rare earth elements. *In*: "Rare Earth Element Geochemistry", P. Henderson, ed. Developments in Geochemistry **2**, Elsevier, Amsterdam-Oxford-New York-Tokyo, 343-373.

Fransolet, A.-M., Kramm, U., Schreyer, W. (1977): Metamorphose und Magmatismus im Venn-Stavelot-Massiv, Ardennen. *Fortschr. Mineral.*, **55**, Beih. 2, 75-103.

Giuseppetti, G., Mazzi, F., Tadini, C. (1991): The crystal structure of monoclinic langbanite: $(Mn,Ca,Fe,Mg)^{2+}{}_4(Mn,Fe)^{3+}{}_9Sb^{5+}[O_{16}(SiO_4)_2]$. *N. Jb. Mineral.*, *Mh.*, 1991, 193-211.

Hanson, A. (1983): Etude minéralogique de filons de la bordure méridionale du massif de Stavelot. Mémoire de Licence, Université de Liège 84pp.

Hawthorne, F.C., Krivovichev, S.V., Burns, P.C. (2000): The crystal chemistry of sulfate minerals. *In*: «Reviews in Mineralogy and Geochemistry», Vol. 40, Sulfate Minerals, Ed. Alpers, C.N., Jambor, J.L., Nordstrom, D.K., Mineralogical Society of America, Geochemical Society, 1-112.

Hoffmann, C., Armbruster, T., Kunz, M. (1997): Structure refinement of (001) disordered gaudefroyite $Ca_4Mn_3^{+3}[BO_3)_3(CO_3)O_3]$: Jahn-Teller-distortion in edge-sharing chains of $Mn^{3+}O_6$ octahedra. *Eur. J. Mineral.*, **9**, 7-19.

Kramm, U. (1979): Kanonaite-rich viridines from the Venn-Stavelot Massif, Belgian Ardennes. *Contrib. Mineral. Petrol*., **69**, 387-395.

— (1982): Die Metamorphose des Venn-Stavelot-Massivs, nordwestliches Rheinisches Schiefergebirge: Grad, Alter und Ursache. *Decheniana (Bonn)*, **135**, 121-178.

Mandarino, J.A. (1981): The Gladstone-Dale relationship: Part IV. The compatibility concept and its application. *Can. Mineral.*, **19**, 441-450.

Moore, P.B., Sen Gupta, P.K., Le Page, Y. (1991): The remarkable långbanite structure type: Crystal structure, chemical crystallography, and relation to some other close-packed structures. *Am. Mineral*., **76**, 1408-1425.

Nickel, E.H. & Grice, J.D. (1998): The IMA Commission on new minerals and mineral names: procedures and guidelines on mineral nomenclature, 1998. *Can. Mineral.*, **36**, 913-926.

Schreyer, W., Fransolet, A. - M., Abraham, K. (1986): A miscibility gap in the trioctahedral Mn-Mg-Fe chlorites: Evidence from the Lienne Valley manganese deposit, Ardennes, Belgium. *Contrib. Mineral. Petrol.*, **94**, 333-342.

Schreyer, W., Fransolet, A.-M., Bernhardt, H.-J. (2001): Hollandite-strontiomelane solid solutions coexisting with kanonaite and braunite in late quartz veins of the Stavelot Massif, Belgium. *Contrib. Mineral. Petrol.*, **141**, 560-571.

Schreyer, W., Bernhardt, H.-J., Fransolet, A.-M., Armbruster, T. (2004): End-member ferrian kanonaite: an andalusite phase with one Al fully replaced by $(Mn, Fe)^{3+}$ in a quartz vein from the Ardennes mountains, Belgium, and its origin. *Contrib. Mineral. Petrol.*, **147**, 276-287.

Starova, G.L., Krivovichev, S.V., Filatov, S.K. (1998): Crystal chemistry of inorganic compounds based on chains of oxocentered tetrahedra. II. Crystal structure of $Cu_4O_2[(As,V)O_4]Cl$. *Zeits. Kristall.*, **213**, 650-653.

Strunz, H. & Nickel, E.H. (2001): Strunz Mineralogical Tables, ninth edition. E. Schweizerbart´sche Verlagsbuchhandlung (Nägele u. Obermiller), Stuttgart, 870pp.

Theunissen, K. & Martin, H. (1969): Découverte d'un phosphate alumineux de terres rares dans un coticule de Vielsalm. *Ann. Soc. Géol. Belgique*, **92**, 173-176.

Verniers, J., Herbosch, A., Vanguestaine, M., Geukens, F., Delcambre, B., Pingot, J.-L., Belanger, I., Hennebert, M., Debacker, T., Sintubin, M., De Vos, W. (2001): Cambrian-Ordovician-Silurian lithostratigraphic units (Belgium). *Geologica Belgica*, **4**, 5-38.

Yvon, K., Jeitschko, W., Parthe, E. (1977): LAZYPULVERIX, a computer program, for calculating X-ray and neutron diffraction powder patterns. *J. Appl. Cryst.*, **10**, 73-74.

Received 27 October 2004
Modified version received 10 March 2005
Accepted 12 April 2005